Biochimica et Biophysica Acta 1797 (2010) 1563–1572

Contents lists available at ScienceDirect

Biochimica et Biophysica Acta

journal homepage: www.elsevier.com/locate/bbabio

Review

Electron flow through metalloproteins

Harry B. Gray *, Jay R. Winkler *

Beckman Institute, California Institute of Technology, Pasadena, CA 91125, USA

ARTICLE INFO

Article history:
Received 10 February 2010
Received in revised form 21 April 2010
Accepted 3 May 2010
Available online 9 May 2010

Keywords:
Electron transfer
Cytochrome *c*
Azurin
Cytochrome b_{562}
Electron tunneling
Electron hopping

ABSTRACT

Electron transfers in photosynthesis and respiration commonly occur between metal-containing cofactors that are separated by large molecular distances. Understanding the underlying physics and chemistry of these biological electron transfer processes is the goal of much of the work in our laboratories. Employing laser flash-quench triggering methods, we have shown that 20 Å, coupling-limited Fe(II) to Ru(III) and Cu(I) to Ru(III) electron tunneling in Ru-modified cytochromes and blue copper proteins can occur on the microsecond timescale both in solutions and crystals; and, further, that analysis of these rates suggests that distant donor–acceptor electronic couplings are mediated by a combination of sigma and hydrogen bonds in folded polypeptide structures. Redox equivalents can be transferred even longer distances by multistep tunneling, often called hopping, through intervening amino acid side chains. In recent work, we have found that 20 Å hole hopping through an intervening tryptophan is several hundred-fold faster than single-step electron tunneling in a Re-modified blue copper protein.

1. Introduction

A great many biological energy transduction pathways depend upon the rapid movement of electrons or holes over long distances (>30 Å) through proteins. Many redox enzymes, particularly those involved in oxygen activation and production, require the transfer of holes at high potentials where the sidechains of redox-active amino acids can become involved. Stringent design requirements must be met to transport charges rapidly and efficiently along specific pathways and prevent the off-path diffusion of redox equivalents and the disruption of energy flow.

Reduction and oxidation (redox) reactions are vital transformations in a wide array of metabolic processes. The mitochondrial respiratory chain of aerobic organisms is among the best characterized of such pathways [1–12]. Reducing equivalents from NADH in the mitochondrial matrix enter the chain in respiratory Complex I. Two equivalents move ~140 Å down a sequence of 7–8 iron–sulfur clusters to reduce a membrane-embedded quinone and translocate four protons across the inner mitochondrial membrane [4,5]. Quinol moves on to the bc_1 complex (respiratory Complex III) where its two reducing equivalents follow a bifurcated pathway [9–11,13]. The first electron moves along a high-potential pathway from a [2Fe–2S] cluster to cytochrome c_1 in a step that likely involves domain movement, then finally to cytochrome *c* in the intermembrane space. The second quinol electron enters a low-potential chain of *b*-type cytochromes and migrates toward the mitochondrial matrix where it participates in the reduction of quinone to quinol, providing energy for proton pumping. Reduced cytochrome *c* diffuses to respiratory Complex IV (cytochrome *c* oxidase) where it delivers electrons to the binuclear Cu_A site [3,6,7]. Electrons from Cu_A move through cytochrome *a* on their way to the cytochrome a_3/Cu_B site of O_2 reduction. Four additional protons are pumped across the inner mitochrondrial membrane by Complex IV as O_2 is reduced to H_2O. The proton gradient generated by proton pumping in Complexes I, III, and IV drives ATP synthesis by Complex V (ATP synthase) [3,12].

Diseases associated with the failure of respiratory chain components are known as mitochondrial encephalomyopathies [1,14,15]. These conditions are characterized by a diverse array of clinical manifestations including defects in the central and peripheral nervous systems, skeletal muscles, eye, blood, endocrine system, heart, gastrointestinal system, kidney, ear, nose, and throat [1,14]. Mitochondrial dysfunction also is implicated in aging whereby mitochondrial DNA (mtDNA) mutations lead to increased production of reactive oxygen species (ROS) which in turn leads to further mtDNA damage [16,17]. Late in life, damaged mtDNA levels can reach the threshold necessary for mitochondrial dysfunction in an organ or tissue, and disease in an individual.

Although hundreds of point mutations and large-scale mtDNA deletions have been associated with particular conditions, the pathogenesis of mtDNA related disorders is not understood [14]. The specific relationships between respiratory electron transfer (ET) reactions and mitochondrial dysfunction are unknown [18]. Complete failure of the respiratory chain, leading to the absence of ATP production, is certainly fatal. But, the consequences of *inefficient*

* Corresponding authors.
E-mail addresses: hbgray@caltech.edu (H.B. Gray), winklerj@caltech.edu (J.R. Winkler).

0005-2728/$ – see front matter © 2010 Published by Elsevier B.V.
doi:10.1016/j.bbabio.2010.05.001

electron flow need not be so catastrophic, particularly given the fact that mtDNA mutations generally are not present in all mtDNA (heteroplasmy) [1,14]. A considerable danger of poor ET in the respiratory chain is the production of ROS which can have deleterious effects on virtually every component of a living cell [19–21].

Oxidative phosphorylation in the respiratory chain is just one of the many redox pathways in aerobic organisms that utilize the oxidizing power of molecular oxygen. One particularly widespread transformation involves hydrogen atom abstraction chemistry. Ribonucleotide reductase, the enzyme responsible for the production of deoxyribonucleic acids, is a case in point [22–26]. This biological redox machine requires a multistep electron tunneling architecture to facilitate the movement of charges rapidly over long distances with only a small loss of free energy. Moreover, the enzyme operates at a very high potential where the sidechains of aromatic amino acids (e.g., tryptophan, tyrosine) are believed to participate in the charge migration process [27]. In *Escherichia coli* ribonucleotide reductase, a hole originating on the Y122 radical is transferred some 35 Å to the active site, retaining sufficient oxidizing power to generate the C439 radical that initiates conversion of nucleotides to deoxynucleotides [22,25,27,28].

A large class of mono-oxygenase enzymes utilizes O_2 to drive C–H activation processes. Prime examples are the cytochromes P450, a group of heme enzymes involved in a vast array of reactions that includes steroid biosynthesis, xenobiotic detoxification, drug metabolism, and carcinogenesis [29–31]. A close relative of P450 is nitric oxide synthase (NOS) [32], an enzyme that catalyzes the synthesis of nitric oxide (•NO) and L-citrulline from L-arginine and O_2 [33]. Owing mainly to the role •NO plays as a signaling molecule in an astonishing number of bodily processes, NOS malfunction is implicated in a large number of diseases [34–38]. Specifically, •NO overproduction by iNOS is involved directly in the pathology of inflammation in diseases such as rheumatoid arthritis, septic shock, atherosclerosis, and diabetes [38,39]. In addition, overexpression of NOS in various types of tumors suggests that the enzyme is upregulated in cancer cells [40]. This observation suggests that NOS could be an important target for the treatment of human tumors. These discoveries about the diverse biological roles of P450 and NOS have brought the enzymes and their catalytic mechanisms into the spotlight as targets of great pharmacological interest [41].

Hydrogen-atom abstraction reactions are believed to be key mechanistic steps in many of the foregoing enzymatic conversions. The high formal reduction potential associated with this process (Eq. (1)) [42,43] highlights the need for a powerful oxidant.

$$R^{\bullet} + H^{+} + e^{-} \rightarrow R{-}H \quad E^{\circ\prime} > 1\ \text{V vs. NHE, pH 7} \tag{1}$$

The complete four-electron reduction of O_2 to H_2O, however, has a potential of just 0.82 V vs. NHE (pH 7, 1 atm O_2) [44] and is not well matched to C-H activation. Consequently, many of the metalloenzymes that catalyze these transformations act by initially reducing O_2 to the H_2O_2 level ($E^{\circ\prime} = 1.35$ V) [44]. In many cases, this reduction process is rate limiting during enzymatic turnover, and the reactive intermediates that actually effect the H-atom abstraction have never been characterized.

Our research program has been designed to elucidate the factors that determine the rates and efficiencies of biological electron flow [45,46]. A key element of our research program has been the development of inter- and intramolecular laser flash-quench methods to trigger ET reactions [45–48]. We have used these methods to study the distance and medium dependences of long-range electron tunneling reactions [45,46], to trigger redox enzyme catalysis [49], and to initiate multistep tunneling processes [50].

2. Electron tunneling

Single electron transfer reactions can be found at the core of most biological redox processes. No fewer than 15 ET reactions, for example, are required to take reducing equivalents from NADH, deposit them in O_2, and generate the electrochemical proton gradient that drives ATP synthesis [3–12]. Most of these reactions involve quantum-mechanical electron tunneling between redox cofactors embedded in protein matrices separated by large molecular distances (>10 Å) [3–12]. The semiclassical theory of ET (Eq. (2)) provides a basic framework for understanding the specific rates of reaction

$$k_{ET} = \sqrt{\frac{4\pi^3}{h^2 \lambda k_B T}} H_{AB}^2 \exp\left\{-\frac{(\Delta G^{\circ} + \lambda)^2}{4\lambda k_B T}\right\} \tag{2}$$

between an electron donor (***D***) and acceptor (***A***) held at fixed distance and orientation (k_{ET}) [45,46,51]. These rates depend on three critical parameters: (1) the driving force for the electron transfer ($-\Delta G^{\circ}$); (2) the extent of nuclear reorientation (λ) in ***D***, ***A***, and solvent that accompanies formation of $\boldsymbol{D}^+$ and $\boldsymbol{A}^-$; and (3) the electronic coupling (H_{AB}) between the reactants [***D***, ***A***] and products [$\boldsymbol{D}^+$, $\boldsymbol{A}^-$] at the transition state. The first two parameters depend largely on the chemical composition and environments of the redox centers, whereas the third is a function of the ***D–A*** distance and the structure of the intervening medium [45,46,51–55].

Several experimental investigations have demonstrated that solvent hole and electron states can mediate long-range electron tunneling [56–61]. In fluid solution, when the positions of **D** and **A** are not constrained by a covalent bridge, diffusion places an upper limit on the timescale ($<10^{-9}$ s) and, therefore, the tunneling distance range (<9 Å for $\beta = 1.0$ Å^{-1}). Longer tunneling distances can be examined if **D** and **A** are immobilized. In a typical experiment, a small concentration of electron or hole donors is embedded in a glassed solvent amid a higher concentration of randomly distributed acceptors. The donor is a photoexcited chromophore or a radiolytically generated radical. The time-dependent survival probability of the donor depends on the concentration of acceptors, the rate constant for electron/hole transfer when **D** and **A** are in van der Waals contact (k_o), and the exponential distance decay factor (β). Extracting reliable values for k_o and β from time-resolved spectroscopic measurements, however, can be rather difficult because the two parameters are highly correlated [61,62]. For the case of photoinitiated ET in glasses, measurements of luminescence decay kinetics and luminescence quantum yields at several different quencher concentrations provide enough information to decouple k_o and β, permitting reliable values to be determined for each parameter [61].

Our experimental investigation of $Ru(tpy)_2^{2+}$ (tpy = 2,2′,2″-terpyridine) luminescence quenching by $Fe(OH_2)_6^{3+}$ in aqueous acidic glasses placed rigorous limits on the distance decay constant for tunneling through water [63]. The luminescence lifetime of $^*Ru(tpy)_2^{2+}$ in aqueous glasses is long enough to allow a significant distance range (~25 Å) to be probed. A distance decay constant of 1.58(5) Å^{-1} was obtained for H_2SO_4/H_2O, HSO_3F/H_2O, and D_2SO_4/D_2O glasses. Distance decay factors can be related to effective tunneling barrier heights (ΔE_{eff}) using standard tunneling models: for electron tunneling through aqueous glasses, $\Delta E_{eff} = 2.4$ eV [46,64].

We also have determined β and ΔE_{eff} values for electron tunneling from electronically excited [Ir(μ-pyrazolyl)(1,5-cyclooctadiene)]$_2$ to 2,6-dichloro-1,4-benzoquinone in 2-methyltetrahydrofuran (MTHF) and toluene glasses at 77 K [64]. The effective barrier height for electron tunneling through toluene ($\Delta E_{eff} = 1.4$ eV) is substantially lower than the barrier in MTHF ($\Delta E_{eff} = 2.6$ eV); and the barrier for tunneling in aqueous sulfuric acid glasses ($\Delta E_{eff} = 2.4$ eV) is very near that for MTHF. Distance decay parameters are 1.62 (MTHF), 1.58

(H_2O), and 1.23 $Å^{-1}$ (toluene) [64]. In toluene and MTHF, coupling between bridge units is mediated by van der Waals contacts, whereas the aqueous glass is interlaced with strong hydrogen bonds. It is possible that the hydrogen bonds between molecules in the aqueous glass compensate for the large HOMO-LUMO (H_2O) energy gap to produce a tunneling barrier on par with that of MTHF.

The 1.62 $Å^{-1}$ distance decay constant for MTHF confirms that there is a significant coupling penalty associated with tunneling across the van der Waals gaps between solvent molecules. Taking 20 Å as a reference distance, we find that tunneling across an alkane bridge ($\beta \sim 1.0$ $Å^{-1}$ [65]) is roughly 40,000 times faster than tunneling through MTHF; and, to underscore the point, recent experiments on **D**-oligoxylene-**A** complexes have shown that 20-Å tunneling across covalently linked xylenes is almost 3000 times faster than tunneling through a toluene glass (Fig. 1) [64].

3. Iron and copper proteins

In 1982, we demonstrated long-range electron tunneling through Ru-modified cytochrome *c* [66]. Subsequent work in our laboratory has focused on the elucidation of distant electronic couplings between redox sites in several Ru-proteins [45,67–71]. In particular, work on Ru-azurin has provided a reference point for electron tunneling through folded polypeptide structures [45,68,69]. The copper center in azurin is situated at one end of an eight-stranded β-barrel, ligated in a trigonal plane by two imidazoles (His46, His117) and a thiolate (Cys112); in addition, there are weak axial interactions (Met121 thioether sulfur, Gly45 carbonyl oxygen) [72,73]. The azurin from *Pseudomonas aeruginosa* has two additional His residues, one of which (His83) reacts readily with Ru-labeling reagents. A H83Q base mutant was prepared and individual mutant His residues were introduced at five locations on β-strands extending from the Cys112 and Met121 ligands (K122H, T124H, T126H, Q107H, M109H) [68,69]. Tunneling distances (Ru-Cu) in these five $Ru(bpy)_2(im)(HisX)^{2+}$-azurins and $Ru(bpy)_2(im)(His83)^{2+}$-azurin range from 16 to 26 Å.

Measurements of Cu(I) → Ru(III) ET ($-\Delta G° = 0.7$ eV) in the set of Ru-azurins established the distance dependence of electron transfer along β-strands [45,68,69]. The driving-force-optimized azurin tunneling timetable reveals a nearly perfect exponential distance dependence, with a decay constant (β) of 1.1 $Å^{-1}$, and an intercept at close contact ($r_o = 3$ Å) of 10^{13} s^{-1} (Fig. 2). Moreover, our studies have shown that Cu(I) to Ru(III) or Os(III) ET rates in labeled azurin crystals are nearly identical with solution values for each donor–acceptor pair [73]. The azurin distance decay constant is quite similar to that found for superexchange-mediated tunneling across saturated alkane bridges ($\beta \approx 1.0$ $Å^{-1}$) [65,74], strongly indicating that a similar coupling mechanism is operative in the polypeptide. Importantly, kinetics data obtained by Farver and Pecht in their studies of long-range ET from radiolytically generated disulfide radical anion to the blue copper center in azurin also have been interpreted successfully in terms of this coupling model [75].

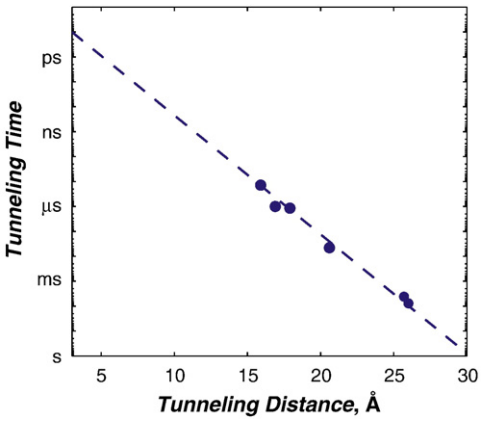

Fig. 2. Distance dependence of driving-force-optimized ET rates in Ru-labeled *P. aeruginosa* azurin. The dashed blue line is the best fit to the data ($\beta = 1.1$ $Å^{-1}$).

The energy gap between the donor/acceptor redox levels and those of oxidized or reduced intermediate states is the primary criterion in determining when hole or electron hopping becomes important [76]. In Ru-azurin, photogenerated $Ru(bpy)_2(im)(His)^{3+}$ ($E° = 1.0$ V vs. NHE) [47] potentially could oxidize Trp or Tyr residues [45]. If the Cu(I) center is replaced by redox-inert Zn(II) in the protein, however, we find that photogenerated holes in $Ru(bpy)_2(im)(HisX)^{3+}$ complexes remain localized on the metal center. The energy gap between the Ru(III) hole and oxidized bridge states must therefore be greater than 75 meV ($3k_BT$ at 295 K). Our finding that the Cu(I) → Ru(III) ET rate in $Ru(bpy)_2(im)(HisX)$-azurin does not decrease in going from 300 to 240 K and actually increases slightly at 160 K demonstrates that hopping does not occur in this case, as a reaction with an endergonic step would be highly disfavored at low temperature. We conclude that the Ru-azurin timetable (Fig. 2) provides a benchmark for superexchange-mediated electron tunneling through proteins.

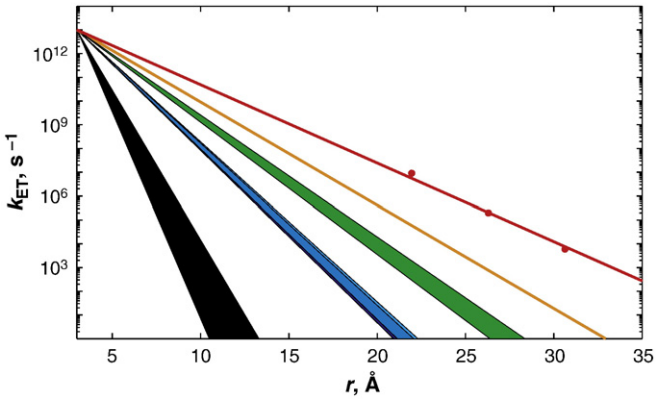

Fig. 1. Distance dependence for electron tunneling through vitreous solvents at 77 K: tetrahydrofuran ($\beta = 1.57$–1.67 $Å^{-1}$, dark blue); aqueous solution (25% H_2SO_4) (1.55–1.65 $Å^{-1}$, cyan); toluene (1.18–1.28 $Å^{-1}$, green). The distance dependences of tunneling through vacuum (2.9–4.0 $Å^{-1}$, black), and across saturated alkane (1.0 $Å^{-1}$, orange), and xylyl (0.76 $Å^{-1}$, red) bridges are shown for comparison [64].

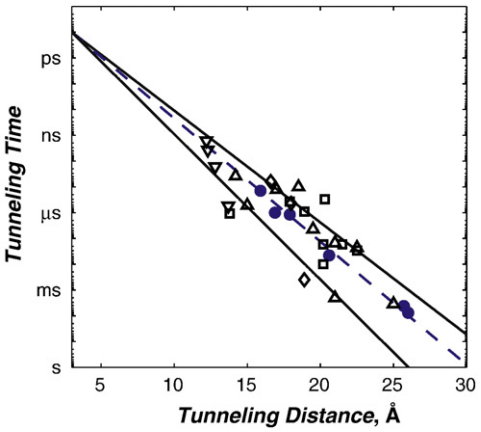

Fig. 3. Tunneling timetable for intraprotein ET in Ru-modified azurin (•), cytochrome *c* (□), myoglobin (◇), cytochrome b_{562} (Δ), HiPIP (▽). The solid black lines illustrate distance decay factors of 1.3 (lower) and 1.0 $Å^{-1}$ (upper); the dashed blue line illustrates a 1.1 $Å^{-1}$ decay.

The rates of high-driving-force ET reactions have been measured for more than 30 Ru(diimine)-labeled metalloproteins (Fig. 3) [45,67,70,77]. Driving-force-optimized values are scattered around the Ru-azurin 1.1 $Å^{-1}$ exponential distance decay. Rates at a single distance can differ by as much as a factor of 10^3 and **D**/**A** distances that differ by as much as 5 Å can produce identical rates. In seminal work, Beratan and Onuchic developed a generalization of the McConnell superexchange coupling model that accounts for rate scatter attributable to protein structural complexity [52,78,79]. In this tunneling-pathway model, the medium between **D** and **A** is decomposed into smaller subunits linked by covalent bonds, hydrogen bonds, or through-space jumps. More elaborate computational protocols also have shed light on the factors that determine distant couplings in proteins [55,80–93].

Empirical data from Ru-modified proteins demonstrate conclusively that long-range electron tunneling rates depend critically on the composition and structure of the medium between two redox centers. The polypeptide matrices of folded proteins are not homogeneous media and consequently electron tunneling rates in proteins do not exhibit uniform exponential distance dependences. It is convenient to characterize the coupling efficiency of a particular polypeptide matrix by an *effective* exponential decay constant (β'). Taking the data in Fig. 3, we can define β' values for each Ru-modified protein, assuming an intercept at close contact ($r_o = 3$ Å) of 10^{13} s^{-1}. The histogram of β' values from Ru-modified proteins (Fig. 4) reveals an asymmetric distribution peaking near 1.1 $Å^{-1}$, with extremes of 0.85 and 1.5 $Å^{-1}$. This range of β' values is entirely consistent with studies of ET in synthetic donor–bridge–acceptor complexes [65,74].

Heterogeneous polypeptide matrices bear some similarities to frozen solvent glasses as electron tunneling media. We have found that decay constants for tunneling through aqueous and tetrahydrofuran glasses (1.6 $Å^{-1}$) are substantially greater than those found for most proteins (Fig. 1). Tunneling across oligoxylene bridges, an all-covalent analogue of glassy toluene (1.2 $Å^{-1}$), is far more efficient (0.75 $Å^{-1}$). It is interesting to note that values of frozen-solvent tunneling rate constants extrapolated to close contact ($0.5–5 \times 10^{13}$ s^{-1}) are in good agreement with that found for Ru-modified azurin. In terms of long-range coupling efficiency, however, frozen solvent glasses are greatly inferior to polypeptide matrices as ET media; the larger β values in solvents are likely a consequence of the predominance of van der Waals contacts over covalent contacts between donors and acceptors.

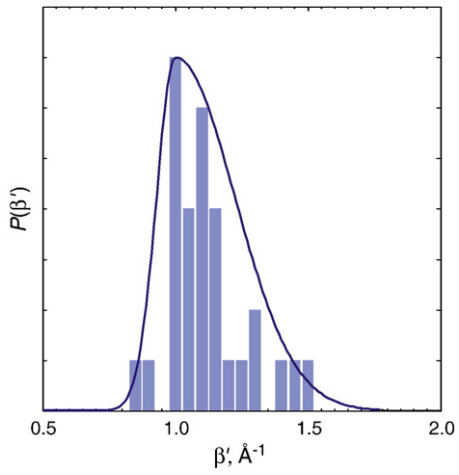

Fig. 4. Histogram of the distribution of distance-decay factors extracted from Ru-protein ET data. The solid blue curve constructed from an asymmetric Gaussian function is an approximate continuous representation of the discrete distribution (light blue bars) derived from the experimental data.

4. ET speed limit

The nonadiabatic ET model embodied in Eq. (2) rests on the assumption that the electronic transition from the reactant potential energy surface (**D** + **A**) to the product surface ($\mathbf{D}^+ + \mathbf{A}^-$) is much slower than the frequency of nuclear motion on these surfaces. Both theoreticians and experimentalists have long been interested in charge-transfer processes that are not well described by this model [94–101]. Theory suggests that, under certain circumstances, the timescales for reorientation of solvent molecules can be slower than the reactant-product transition frequency. In this solvent-controlled adiabatic limit, reactions are limited by the dynamics of solvent relaxation. Theoretical rate expressions have been developed to account explicitly for solvent relaxation dynamics (Eqs. (3)–(4)) [94,100,101]. The parameter κ is a solvent adiabaticity factor and k_{NA} is the nonadiabatic ET rate constant given by Eq. (2).

$$k = \frac{k_{NA}}{1 + \kappa} \tag{3}$$

$$\kappa = \frac{2\pi H_{AB}^2 \langle\tau\rangle}{\hbar\lambda_o} \tag{4}$$

Small values of κ correspond to the nonadiabatic limit; large values result in solvent-controlled adiabatic processes. Typical solvent relaxation times ($\langle\tau\rangle$) are $\leq 10^{-11}$ s, so that solvent relaxation dynamics are expected to become important only in relatively strongly coupled systems. An adiabaticity factor of 1 in a solvent with a 1-ps relaxation time, for example, corresponds to a coupling matrix element of ~60 cm^{-1} ($\lambda_o = 0.5$ eV).

Our studies of ET in Ru-proteins indicate that a large part of the contribution to λ_o comes from reorientation of the polypeptide matrix [73]. The dynamics of large scale nuclear motions in polypeptides are expected to be substantially slower than those of most solvents. Relaxation times ranging from picoseconds to microseconds have been reported for the heme pocket of myoglobin [102–105]. Indeed, electrochemical measurements by Waldeck and coworkers using cytochrome *c* adsorbed onto self-assembled monolayers suggest that the characteristic relaxation time for protein electron transfer is on the order of 200 ns [106]. We emphasize, however, that eight tunneling times measured for four different Ru-proteins are shorter than 200 ns (Fig. 3).

Bixon and Jortner [107,108] have noted that there are several examples of ET rates exceeding the solvent-controlled adiabatic limit; model calculations suggest a possible explanation. Reactions at low driving force ($-\Delta G^\circ \ll \lambda$) require substantial reorganization along solvent coordinates and rates are predicted to exhibit a pronounced dependence on relaxation dynamics. The calculations suggest, however, that the rates of activationless ($-\Delta G^\circ \sim \lambda$) and inverted ($-\Delta G^\circ > \lambda$) reactions will be nearly independent of κ and, hence, the dynamics of medium relaxation, as we have found in the case of Ru-(diimine)-protein ET reactions [45].

The intercept of 10^{13} s^{-1} at $r_o = 3$ Å represents the "ET speed limit"; it is the specific rate expected for coupling-limited ET between two redox centers in van der Waals contact. Direct comparisons between this extrapolated value and ultrafast ET data are complicated by the effects of medium dynamics: as donor–acceptor electronic coupling increases, a regime is reached where rates are no longer limited by the strength of this coupling, but by the dynamics of solvent reorientation, as discussed above. This so-called solvent controlled adiabatic limit will typically be below the nonadiabatic limiting rate constant (k_{NA}) determined by extrapolation of rate-distance data to a close-contact intercept.

Consider two model systems that provide insights into limiting ET rates at close contact. Barbara and coworkers examined thermal ET following metal-to-metal charge transfer (MMCT) excitation in

$(NH_3)_5Ru^{III}NCM^{II}(CN)_5^-$ (M = Fe, Ru) [109,110]. These mixed-valence complexes fall in the Robin-Day Class II category [111]; the MMCT extinction coefficients are $\sim 3\times10^3$ $M^{-1}cm^{-1}$ and the estimated electronic coupling parameters are 1900 (M = Ru) and 1500 cm^{-1} (M = Fe) [109]. In solvents with relatively fast dielectric relaxation (*e.g.*, H_2O, formamide, N-methyl-formamide), observed $Fe^{II}\rightarrow Ru^{III}$ and $Ru^{II}\rightarrow Ru^{III}$ ET rate constants are $\sim 10^{13}$ s^{-1}. Solvent relaxation dynamics typically are divided into two distinct timescales: fast components corresponding to inertial motions of the solvent occur in tens of femtoseconds; and slow processes (>0.5 ps) corresponding to overdamped motions. Because ET in $(NH_3)_5Ru^{III}NCM^{II}(CN)_5^-$ is faster than slow solvent relaxation components, Barbara concluded that overdamped solvent motions play only a minor role in the ultrafast reaction [109,110]. Hence, in these binuclear metal complexes, specific ET rates are $\sim 10^{13}$ s^{-1} at a metal–metal separation of ~5 Å [112]. The path between the two metals is fully covalent, so the coupling should be greater than that for two centers in van der Waals contact.

Photoinitiated ET in charge transfer (CT) complexes provides a second comparison to our extrapolated maximum rate constant. Spears and coworkers examined viologen (methyl viologen, MV; heptyl viologen, HV) complexes with 4,4′-biphenol (BP) [113]. The noncovalent interaction between the two redox groups is weaker than in the bimetallic complexes; the CT extinction coefficients are $\sim 4\times10^1$ $M^{-1}cm^{-1}$ and the estimated electronic coupling parameters are 361 (MV) and 381 cm^{-1} (HV). *Ab initio* calculations of the optimum ground-state geometry in the MV-BP complex suggest a 4 Å separation between planes of the aromatic rings. The specific thermal ET rates following ultrafast excitation into the CT absorption band in fast-relaxing solvents (e.g., methanol, acetonitrile) are $\sim 2.5\times10^{12}$ s^{-1}. Each of these ET reactions likely falls in the solvent-controlled adiabatic limit; the estimated specific rate in the absence of solvent control is 2.5×10^{13} s^{-1} [113].

Results of the foregoing ultrafast ET experiments are consistent with the k_{ET} value (10^{13} s^{-1}) extrapolated to close contact between redox sites in Ru-azurins. The separation distance at which this limit is achieved depends on whether the two sites are covalently coupled or are in van der Waals contact. In the case of intraprotein ET between two metal complexes (i.e., $Ru(bpy)_2(im)(HisX)^{3+}$ and Cu(His46)(His117)(Cys112)(Met121)$^+$), we believe that van der Waals contact between the two metal centers, not the metal–ligand complexes, is more consistent with an ET rate of 10^{13} s^{-1}. Hence, in our analyses of protein ET rates, we consider metal-to-metal distances with a contact separation of 3 Å.

5. Multistep electron tunneling (hopping)

Electron tunneling times must be in the millisecond to microsecond range for biological redox machines to function properly. As a result, the maximum center-to-center distance for single-step tunneling through proteins can be no greater than ~20 Å (Fig. 3). The structures of several redox enzyme assemblies, however, suggest that charge transport may occur over distances that far exceed this single-step limit [22,25,45]. How can charge transport in proteins cover distances well over 20 Å? One possibility is by hopping, as it can be shown that coupled tunneling reactions, particularly with endergonic steps, can in favorable cases deliver electrons or holes rapidly to very distant sites [22,25,27,28,45,70,114–117]. Requirements for functional hopping include optimal positioning of redox centers and fine tuning of reaction driving forces.

Modeling the kinetics of electron hopping is a straightforward problem that can be solved analytically without employing simplifying approximations [45]. Using the well defined properties of ET reactions (Eq. (2)), and the average distance dependence defined by Ru-protein tunneling timetables, it is possible to predict hopping rates for any set of driving-force, temperature, and distance parameters. Consider the two-step tunneling reaction defined in (Eq. (5)) (reactants, $\boldsymbol{R}$ = **D–I–A**; redox intermediate, $\boldsymbol{H}$ = $\mathbf{D^+}$-$\mathbf{I^-}$–**A** or **D**–$\mathbf{I^+}$–$\mathbf{A^-}$; products, $\boldsymbol{P}$ = $\mathbf{D^+}$–**I**–$\mathbf{A^-}$).

$$R \underset{k_{HR}}{\overset{k_{RH}}{\rightleftarrows}} H \underset{k_{PH}}{\overset{k_{HP}}{\rightleftarrows}} P \tag{5}$$

The general solution to the rate law for this process calls for biexponential production of $\boldsymbol{P}$, although under some circumstances the appearance of $\boldsymbol{P}$ can be approximated by a single exponential function. Taking a value of λ = 0.8 eV for both tunneling reactions (*i.e.*, $\boldsymbol{R}\rightarrow\boldsymbol{H}$ and $\boldsymbol{H}\rightarrow\boldsymbol{P}$) and a distance decay constant of 1.1 $Å^{-1}$, we can calculate the time dependence of the populations of all three reacting species for various values of $\Delta G^\circ_{\mathbf{RH}}$, $\Delta G^\circ_{\mathbf{HP}}$, $r_{\mathbf{RH}}$, and $r_{\mathbf{HP}}$ [45]. Results for the particular case in which $\Delta G^\circ_{\mathbf{RH}} = -\Delta G^\circ_{\mathbf{HP}}$ and $r_{\mathbf{RH}} = r_{\mathbf{HP}}$ are illustrated in Fig. 5. This model approximates biological electron transport ($\Delta G^\circ_{\mathbf{RP}} = 0$) with a single endergonic step. Transport across 20 Å is 10^4 times faster than a single tunneling step at this distance and submillisecond transfers can be realized. An important conclusion is that hopping can facilitate electron flow over distances greater than 20 Å in cases where the free-energy changes for endergonic intermediate steps are no greater than 0.2 eV.

We expressed three mutant azurins to test the proposition that an intervening tryptophan or tyrosine can facilitate electron transfer between distant metal redox centers. In these mutants, a histidine ligand is at position 124 on the β strand extending from Met121, and either tryptophan, tyrosine, or phenylalanine is at position 122. The construction was completed by attaching the sensitizer $Re^I(CO)_3$(4,7-dimethyl-1,10-phenanthroline) ($Re^I(CO)_3$(dmp)) to His124. $Re^I(CO)_3$(dmp)(His124) is a powerful oxidant in its ^{3}MLCT excited state: $E^\circ[^*Re^{II}(CO)_3(dmp^{\bullet-})(His124)/Re^I(CO)_3(dmp^{\bullet-})(His124)] = 1.4$ V vs. NHE [118]. The crystal structure of the Re-labeled Trp122 variant ($Re^I(CO)_3$(dmp)(His124)|(Trp122)|$AzCu^{II}$) revealed that dmp and the Trp122 indole group are near van der Waals contact (~4 Å), and the Cu-Re distance is 19.4 Å (Fig. 6) [50].

A combination of time-resolved optical (Fig. 7) and infrared spectroscopy was used to characterize the ET kinetics in this protein. Optical excitation of $Re^I(CO)_3$(dmp)(His124) creates a ^{1}MLCT excited state, which undergoes ~150 fs intersystem crossing [119] to a vibrationally excited triplet (*^{3}MLCT). Subpicosecond generation of $Re^I(CO)_3(dmp^{\bullet-})$(His124) is attributable to ET from Trp122 to the Re^I

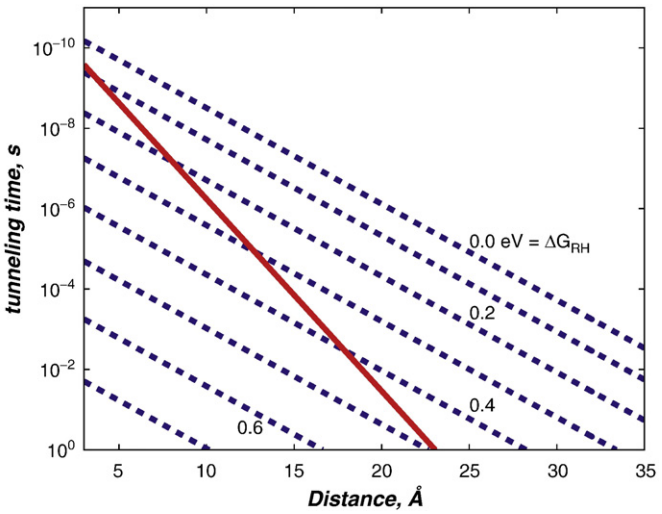

Fig. 5. Distance dependences of the rates of single-step and two-step electron tunneling reactions. Solid red line indicates theoretical distance dependence for a single-step, ergoneutral ($\Delta G^\circ_{RP} = 0$) tunneling process ($\beta = 1.1$ $Å^{-1}$). Dashed blue lines indicate distance dependence calculated for two-step ergoneutral tunneling R⇄H⇄P with the indicated standard free-energy changes for the R⇄H step.

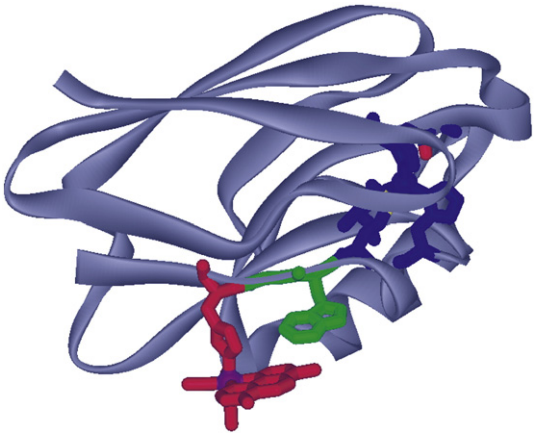

Fig. 6. Model of the Cu-W-Re electron-tunneling architecture from the 1.5 Å resolution x-ray crystal structure of $Re^{I}(CO)_3(dmp)(His124)|(Trp122)|AzCu^{II}$. The aromatic rings of dmp (red) and Trp122 (green) slightly overlap, with one dmp methyl group projecting over the indole ring and the plane of the respective π-systems making a 20.9° angle. The average separation of atoms on the overlapped six-membered rings is 3.82 Å, whereas 4.1 Å separates the edge of the Trp122 indole and the His124 imidazole. Distances between redox centers: Cu (blue) to Trp122 aromatic centroid, 11.1 Å; Trp122 aromatic centroid to Re (purple), 8.9 Å; Cu to Re, 19.4 Å.

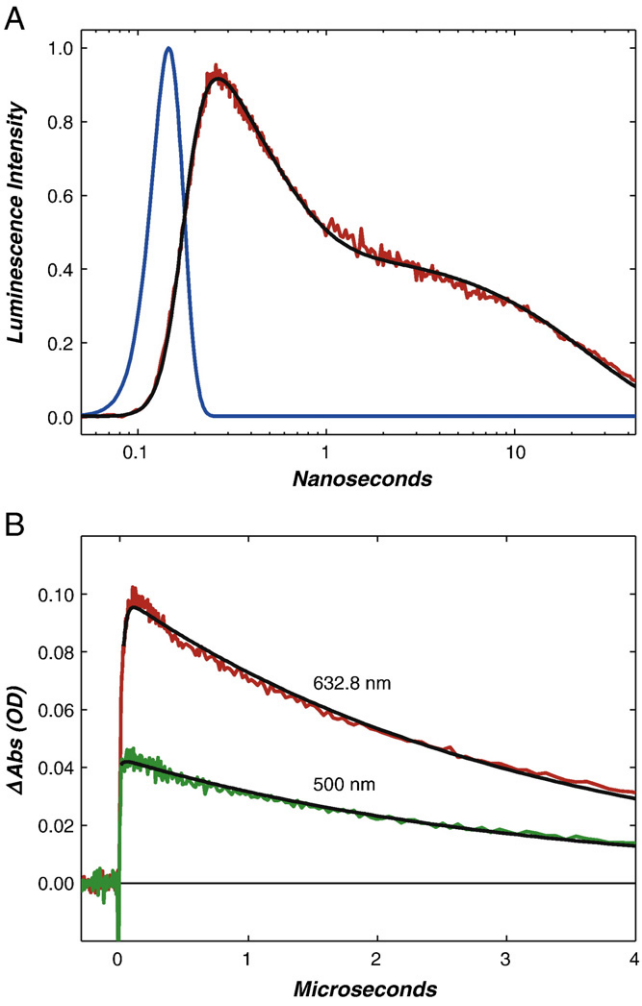

Fig. 7. Transient kinetics of $Re^{I}(CO)_3(dmp)(His124)|(Trp122)|AzCu^{I}$. (A) Time-resolved luminescence (red: λ_{obs}>450 nm; λ_{ex} = 355 nm, 10 ps pulsewidth; pH 7.2), instrument response function (blue), and fit to a three-exponential kinetics model [black: τ_1 = 35 ps (growth); τ_2 = 363 ps (decay); τ_3 = 25 ns (decay)]. (B) Visible transient absorption [λ_{obs} = 632.8 (red), 500 nm (green); λ_{ex} = 355 nm, 1.5 mJ, 8 ns pulsewidth; pH 7.2]. Black lines are fits to a biexponential kinetics model [τ_1 = 25 ns (growth); τ_2 = 3.1 ms (decay)].

$(CO)_3(dmp)(His124)$ excited singlet (^{1}MLCT). A 350-ps kinetics phase is due to equilibration between the ^{3}MLCT state and $Re^{I}(CO)_3(dmp^{\bullet-})(His124)|(Trp122)^{\bullet+}|AzCu^{I}$, and a subsequent 30-ns process to reduction of $(Trp122)^{\bullet+}$ by $AzCu^{I}$ to generate $Re^{I}(CO)_3(dmp^{\bullet-})(His124)|(Trp122)|AzCu^{II}$. Ground-state repopulation proceeds in 3 μs via single-step long-range ET from $Re^{I}(CO)_3(dmp^{\bullet-})(His124)$ to $AzCu^{II}$. Rate constants corresponding to elementary reaction steps were extracted using a numerical procedure to fit all of the time-resolved data to a two-step tunneling kinetics model.

The key finding is that Cu^{I} oxidation in $Re^{I}(CO)_3(dmp)(His124)|(Trp122)|AzCu^{I}$ is more than two orders of magnitude faster than expected for electron tunneling over 19 Å. Analysis of the reaction kinetics revealed that the reduction potential of $^*Re^{II}(CO)_3(dmp^{\bullet-})(His124)$ is just 28 mV greater than that of $(Trp122)^{\bullet+/0}$, but this is sufficient for very rapid (~ns) ET between adjacent dmp and Trp122 aromatic rings. Replacement of Trp122 by Tyr or Phe inhibits the initial ET event, presumably because the $(Tyr122)^{\bullet+/0}$ and $(Phe122)^{\bullet+/0}$ potentials are more than 200 mV above $E°(^*Re^{II}(CO)_3(dmp^{\bullet-})(His124)/Re^{I}(CO)_3(dmp^{\bullet-})(His124))$. Concerted oxidation and deprotonation of Tyr122 by $^*Re^{II}(CO)_3(dmp^{\bullet-})(His124)$ could be thermodynamically favorable, but likely would be accompanied by a significant activation barrier. The Trp radical cation is a relatively weak acid (pK_a = 4.5(2)) [120,121]; its deprotonation, which is energetically favorable at pH 7, likely would proceed on a microsecond timescale [115]. Hence, $(Trp122)^{\bullet+}$ can rapidly oxidize Cu^{I} in the azurin active site as it remains protonated in the hopping intermediate.

We constructed a hopping map of driving-force effects on two-step (Cu^{I} → Int → *ML) and single-step (Cu^{I} → *ML) tunneling rates for a molecular framework analogous to $Re^{I}(CO)_3(dmp)(His124)|(Trp122)|AzCu^{I}$ (Fig. 8). The bounded region in the map corresponds to driving-force regimes in which two-step hopping is faster than single-step tunneling. Our analysis indicates that the overall charge separation rate is more sensitive to the free-energy change for the first of the two tunneling steps. Indeed, the rate advantage of the multistep process is lost if the first tunneling step is too endergonic ($\Delta G°$(Int → *ML) > 200 meV) [45,46]. The map predicts a ~100-ns time constant for Cu^{I} oxidation, in good agreement with the experimental value of ~30 ns. Strikingly, two-step hopping is over 300 times faster than single-step Cu^{I} to $^*Re^{II}(CO)_3(dmp^{\bullet-})(His124)$ tunneling.

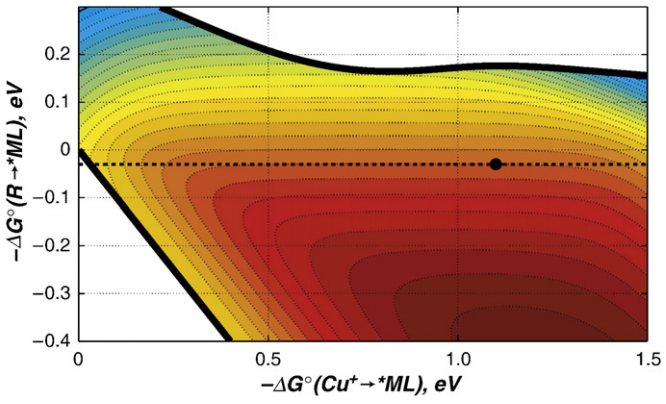

Fig. 8. Two-step hopping map for electron tunneling through Re^{I}-modified azurin. Colored contours reflect electron-transport timescales as functions of the driving force for the first tunneling step (ordinate, Int → *ML) and the overall electron-transfer process (abscissa, Cu^{I} → *ML). The heavy black lines enclose the region in which two-step hopping is faster than single-step tunneling. The dashed black line indicates the driving force for $^*Re^{II}(CO)_3(dmp^{\bullet-})(His124)|(Trp122)|AzCu^{I} \rightarrow Re^{I}(CO)_3(dmp^{\bullet-})(His124)|(Trp122)^{\bullet+}|AzCu^{I}$ ET; the black dot corresponds to $^*Re^{II}(CO)_3(dmp^{\bullet-})(His124)|(Trp122)|AzCu^{I} \rightarrow Re^{I}(CO)_3(dmp^{\bullet-})(His124)|(Trp122)^{\bullet+}|AzCu^{I} \rightarrow Re^{I}(CO)_3(dmp^{\bullet-})(His124)|(Trp122)|AzCu^{II}$ hopping.

6. Protein–protein reactions

At least three elementary steps are required to complete a redox reaction between soluble proteins: (i) formation of an active donor–acceptor complex; (ii) electron tunneling within the donor–acceptor complex; and (iii) dissociation of the oxidized and reduced products. Because the dynamics of the first and third steps obscure the electron tunneling reaction, experimental studies must focus on ET reactions within protein–protein complexes that form at low ionic strength. It has been difficult to interpret the results, however, as neither the donor–acceptor docking geometries nor the conformations of these complexes are known with certainty. With the aid of rapid triggering methods, it has been possible to measure rates of long-range ET between redox sites in protein–protein complexes [122–131]. In many complexes, there are multiple binding sites and it is not uncommon to find that the ET kinetics often are regulated by the dynamics of conformational changes in the complex[132,133]. The usual interpretation is that surface diffusion of the two proteins produces a transient complex with enhanced electronic coupling and faster electron transfer. Consequently, rates depend strongly on solvent viscosity rather than intrinsic ET parameters. A further complication associated with studies of protein–protein ET in solution is that binding sites and, hence, locations of redox cofactors, often are unknown.

Crystals containing photoactivatable donors and acceptors at specific lattice sites are ideal media for investigating tunneling between proteins. In crystal lattices of tuna cytochrome *c*, chains of protein molecules form helices with a 24.1-Å separation between neighboring metal centers [134]. By doping Zn-cyt *c* into this lattice, interprotein ET between triplet-excited Zn-porphyrin and a neighboring Fe(III)-cyt *c* could be investigated; the rate constant was found to be $4(1)\times10^{2}\ s^{-1}$, and charge recombination was about four times faster ($2.0(5)\times10^{3}\ s^{-1}$) [134].

Rapid relay of electrons involving at least one soluble redox enzyme requires the formation of short-lived, weakly bound protein–protein complexes. The recognition sites between proteins in such complexes tend to be smaller (<1200 Å^2) and include more water molecules than the interfaces between subunits in oligomeric proteins [135]. The interprotein interactions in crystals of tuna cyt *c* involve relatively few contacts: 760 Å^2 of surface area is buried in an interface with 31 van der Waals contacts ($3.2\le d\le3.9$ Å) and 16 water molecules (3 of which form bridging hydrogen bonds across the interface) but only one direct hydrogen bond bridging the two proteins. Indeed, the cyt *c* - cyt *c* interface is reminiscent of that between natural redox partners, e.g., cyt *c* and cytochrome *c* peroxidase (770 Å^2) [136], or cyt c_2 and the photosynthetic reaction center [137]. Our finding that ET rates in Zn-doped tuna cyt *c* crystals fall well within the protein range in the Ru-protein tunneling timetable (Fig. 3) [45,134] demonstrates that small interaction zones of low density are quite effective in mediating interprotein redox reactions.

In the terminal reaction of the respiratory chain, cytochrome *c* oxidase (C*c*O) removes electrons from cyt *c* and passes them on to O_2 [138]. C*c*O is a multisubunit membrane-bound enzyme with four redox cofactors (Cu_A, cytochrome *a*, cytochrome a_3, Cu_B). The locations of these metal complexes in C*c*O were revealed in the 1990 s by the x-ray crystal structures of bacterial [7] and bovine enzymes [6,139]. Cu_A, a binuclear site with bridging S(Cys) atoms, is the primary electron acceptor from cyt *c*. Studies with Ru-modified cytochrome *c* reveal rapid ($6\times10^{4}\ s^{-1}$) [140] electron injection from Fe(II) into Cu_A at low driving force ($\Delta G^\circ=-0.03$ eV) [141]. Modeling suggests that cyt *c* binds to the enzyme at an acidic patch on subunit II [142,143]. The cyt *c* heme is very near the Trp104 (subunit II) indole ring, a residue that appears from mutagenesis experiments to be critical for rapid cyt $c\rightarrow Cu_A$ ET [144–147]. Solomon and coworkers have identified a possible electron tunneling path from this cyt *c* binding site through Trp104 to the bridging S(Cys200) ligand on Cu_A [148].

The 19.6 Å electron transfer from Cu_A to cyt *a* proceeds rapidly at low driving force ($\sim10^{4}\ s^{-1}$; $\Delta G^\circ\sim-0.05$ eV) [140,149]. Ramirez [138], Regan [150], and Solomon [148,151] have identified a coupling route that proceeds from Cu_A ligand His204 (subunit II) across one hydrogen bond to Arg438 (subunit I) (H204(Nε)-R438(O), 3.36 Å), and another H-bond (2.95 Å) from the Arg438 N-amide to the cyt *a* heme propionate. Based on a tunneling currents analysis, Stuchebrukhov suggested a slightly different Cu_A to cyt *a* coupling route through His204 [152]. It is likely that, owing to strong Cu-S(Cys) electronic interactions, pathways involving the bridging Cys residues are important for mediating coupling even though they involve more bonds than the His204 route. One possibility is that the sequence Cys200/Ile199/Arg439/heme-propionate (cyt *a*) is the dominant Cu_A to cyt *a* electron tunneling pathway [148,152].

Both Regan [150] and Stuchebrukhov [152] have identified pathways between cyt *a* and cyt a_3. Included among these routes is a direct covalent pathway from the heme-*a* axial ligand His378 through Phe377 to the a_3 His376. Importantly, although the Cu_A-cyt a_3 distance (22.4 Å) is similar to that of Cu_A to cyt *a*, neither Regan [150] nor Stuchebrukhov [152] found a coupling pathway that would facilitate electron flow to a_3 in a single step from the binuclear copper center.

7. Concluding remarks

Activity in the electron tunneling field over the last 20 years has been intense, most especially on the experimental side, where investigators have elucidated many of the factors that control reaction rates through bonded as well as nonbonded atoms in molecules and molecular assemblies, including the important case of folded polypeptide structures.

The field is booming, as tunneling-related solar-cell, sensor, and other device technologies are being developed at a rapid pace. A critical issue here is understanding bridge energy effects on charge transport through molecular materials [153]. The role of dynamics in protein electron transfer is another hot topic these days [82, 133]. Distant (>20 Å) charge transport in DNA is still another area of great interest. Recent work suggests that guanine radicals, which facilitate iron-sulfur cluster oxidation in a DNA/MutY complex, may stimulate DNA repair [154].

Controlled electron flow is an absolute requirement for efficient storage and conversion of all forms of energy. It also is essential for successful operation of molecular-scale electronic devices. We have laid a firm foundation for these applications; but we must greatly ramp up both theoretical and experimental investigations of multi-electron and other coupled redox processes if we are to realize the full potential of this simplest of chemical reactions.

Acknowledgments

Our work is supported by NIH, NSF, and the Arnold and Mabel Beckman Foundation.

References

[1] S. DiMauro, E.A. Schon, Mechanisms of disease: mitochondrial respiratory-chain diseases, N Engl J. Med. 348 (2003) 2656–2668.
[2] G. Lenaz, M.L. Genova, Kinetics of integrated electron transfer in the mitochondrial respiratory chain: random collisions vs. solid state electron channeling, Am. J. Physiol. Cell Physiol. 292 (2007) C1221–C1239.
[3] M. Saraste, Oxidative phosphorylation at the fin de siecle, Science 283 (1999) 1488–1493.
[4] P. Hinchliffe, L.A. Sazanov, Organization of iron–sulfur clusters in respiratory complex I, Science 309 (2005) 771–774.
[5] L.A. Sazanov, P. Hinchliffe, Structure of the hydrophilic domain of respiratory complex I from *Thermus thermophilus*, Science 311 (2006) 1430–1436.

[6] T. Tsukihara, H. Aoyama, E. Yamashita, T. Tomizaki, H. Yamaguchi, K. Shinzawa-Itoh, R. Nakashima, R. Yaono, S. Yoshikawa, Structures of metal sites of oxidized bovine heart cytochrome *c* oxidase at 2.8 Å, Science 269 (1995) 1071–1074.

[7] S. Iwata, C. Ostermeier, B. Ludwig, H. Michel, Structure at 2.8 Å resolution of cytochrome *c* oxidase from *Paracoccus denitrificans*, Nature 376 (1995) 660–669.

[8] F. Sun, X. Huo, Y.J. Zhai, A.J. Wang, J.X. Xu, D. Su, M. Bartlam, Z.H. Rao, Crystal structure of mitochondrial respiratory membrane protein complex II, Cell 121 (2005) 1043–1057.

[9] Z.L. Zhang, L.S. Huang, V.M. Shulmeister, Y.I. Chi, K.K. Kim, L.W. Hung, A.R. Crofts, E.A. Berry, S.H. Kim, Electron transfer by domain movement in stockbroker bc_1, Nature 392 (1998) 677–684.

[10] D. Xia, C.A. Yu, H. Kim, J.Z. Xian, A.M. Kachurin, L. Zhang, L. Yu, J. Deisenhofer, Crystal structure of the cytochrome bc_1 complex from bovine heart mitochondria, Science 277 (1997) 60–66.

[11] S. Iwata, J.W. Lee, K. Okada, J.K. Lee, M. Iwata, B. Rasmussen, T.A. Link, S. Ramaswamy, B.K. Jap, Complete structure of the 11-subunit bovine mitochondrial cytochrome *bc*1 complex, Science 281 (1998) 64–71.

[12] J.P. Abrahams, A.G.W. Leslie, R. Lutter, J.E. Walker, Structure at 2.8-Angstrom resolution of F1-Atpase from bovine heart-mitochondria, Nature 370 (1994) 621–628.

[13] D. Xia, L. Esser, L. Yu, C.A. Yu, Structural basis for the mechanism of electron bifurcation at the quinol oxidation site of the cytochrome bc_1 complex, Photosynth. Res. 92 (2007) 17–34.

[14] S. DiMauro, E.A. Schon, Mitochondrial disorders in the nervous system, Annu. Rev. Neurosci. 31 (2008) 91–123.

[15] R. Janssen, L.G. Nijtmans, L.P. van den Heuvel, J.A.M. Smeitink, Mitochondrial complex I: structure, function and pathology, J. Inherit. Metab. Dis. 29 (2006) 499–515.

[16] A. Navarro, A. Boveris, The mitochondrial energy transduction system and the aging process, Am. J. Physiol. Cell Physiol. 292 (2007) C670–C686.

[17] A. Navarro, J.M. Lopez-Cepero, M.J. Bandez, M.J. Sanchez-Pino, C. Gomez, E. Cadenas, A. Boveris, Hippocampal mitochondrial dysfunction in rat aging, Am. J. Physiol. Regul. Integr. Comp. Physiol. 294 (2008) R501–R509.

[18] D.M. Kirby, D.R. Thorburn, Approaches to finding the molecular basis of mitochondrial oxidative phosphorylation disorders, Twin Res. Hum. Genet. 11 (2008) 395–411.

[19] B. Halliwell, Reactive oxygen species in living systems: source, biochemistry, and role in human disease, Am. J. Med. 91 (1991) 14S–22S.

[20] B. Halliwell, Reactive oxygen species and the central nervous system, J. Neurochem. 59 (1992) 1609–1623.

[21] E.R. Stadtman, B.S. Berlett, Reactive oxygen-mediated protein oxidation in aging and disease, Drug Metab. Rev. 30 (1998) 225–243.

[22] B.M. Sjöberg, Ribonucleotide reductases—a group of enzymes with different metallosites and a similar mechanism, Struct. Bond. 88 (1997) 139–173.

[23] J.M. Bollinger, Biochemistry—electron relay in proteins, Science 320 (2008) 1730–1731.

[24] J.M. Bollinger Jr., D.E. Edmondson, B.H. Huynh, J. Filley, J.R. Norton, J. Stubbe, Mechanism of assembly of the tyrosyl radical–dinuclear iron cluster cofactor of ribonucleotide reductase, Science 253 (1991) 292–298.

[25] J. Stubbe, D.G. Nocera, C.S. Yee, M.C.Y. Chang, Radical initiation in the Class I ribonucleotide reductase: long-range proton-coupled electron transfer? Chem. Rev. 103 (2003) 2167–2201.

[26] J. Stubbe, Di-iron-tyrosyl radical ribonucleotide reductases, Curr. Opin. Chem. Biol. 7 (2003) 183–188.

[27] J. Stubbe, W.A. van der Donk, Protein radicals in enzyme catalysis, Chem. Rev. 98 (1998) 705–762.

[28] M.C.Y. Chang, C.S. Yee, D.G. Nocera, J. Stubbe, Site-specific replacement of a conserved tyrosine in ribonucleotide reductase with an aniline amino acid: a mechanistic probe for a redox-active tyrosine, J. Am. Chem. Soc. 126 (2004) 16702–16703.

[29] F. Hannemann, A. Bichet, K.M. Ewen, R. Bernhardt, Cytochrome P450 systems—biological variations of electron transport chains, Biochim. Biophys. Acta, Gen. Subj. 1770 (2007) 330–344.

[30] S.G. Sligar, T.M. Makris, I.G. Denisov, Thirty years of microbial P450 monooxygenase research: peroxo-heme intermediates—the central bus station in heme oxygenase catalysis, Biochem. Biophys. Res. Commun. 338 (2005) 346–354.

[31] C.M. Brown, B. Reisfeld, A.N. Mayeno, Cytochromes p450: a structure-based summary of biotransformations using representative substrates, Drug Metab. Rev. 40 (2008) 1–100.

[32] A.C.F. Gorren, B. Mayer, Nitric-oxide synthase: a cytochrome P450 family foster child, Biochim. Biophys. Acta, Gen. Subj. 1770 (2007) 432–445.

[33] D.J. Stuehr, Mammalian nitric oxide synthases, Biochim. Biophys. Acta, Bioenerg. 1411 (1999) 217–230.

[34] H.J. Luth, M. Holzer, U. Gartner, M. Staufenbiel, T. Arendt, Expression of endothelial and inducible NOS-isoforms is increased in Alzheimer's disease, in APP23 transgenic mice and after experimental brain lesion in rat: evidence for an induction by amyloid pathology, Brain Res. 913 (2001) 57–67.

[35] H.J. Luth, M. Holzer, H.J. Gertz, T. Arendt, Aberrant expression of nNOS in pyramidal neurons in Alzheimer's disease is highly co-localized with p21(ras) and p16(INK4a), Brain Res. 852 (2000) 45–55.

[36] K.M. Kendrick, R. Guevara-Guzman, J. Zorrilla, M.R. Hinton, K.D. Broad, M. Mimmack, S. Ohkura, Formation of olfactory memories mediated by nitric oxide, Nature 388 (1997) 670–674.

[37] P.L. Huang, Z.H. Huang, H. Mashimo, K.D. Bloch, M.A. Moskowitz, J.A. Bevan, M.C. Fishman, Hypertension in mice lacking the gene for endothelial nitric-oxide synthase, Nature 377 (1995) 239–242.

[38] A.D. Hingorani, J. Cross, R.K. Kharbanda, M.J. Mullen, K. Bhagat, M. Taylor, A.E. Donald, M. Palacios, G.E. Griffin, J.E. Deanfield, R.J. MacAllister, P. Vallance, Acute systemic inflammation impairs endothelium-dependent dilation in humans, Circulation 102 (2000) 994–999.

[39] F. Aktan, iNOS-mediated nitric oxide production and its regulation, Life Sci. 75 (2004) 639–653.

[40] B. Fitzpatrick, M. Mehibel, R.L. Cowen, I.J. Stratford, iNOS as a therapeutic target for treatment of human tumors, Nitric Oxide Biol. Chem. 19 (2008) 217–224.

[41] A.S. Kalgutkar, R.S. Obach, T.S. Maurer, Mechanism-based inactivation of cytochrome P450 enzymes: chemical mechanisms, structure–activity relationships and relationship to clinical drug-drug interactions and idiosyncratic adverse drug reactions, Curr. Drug Metab. 8 (2007) 407–447.

[42] K.A. Gardner, J.M. Mayer, Understanding C–H bond oxidations: H and H^+ transfer in the oxidation of toluene by permanganate, Science 269 (1995) 1849–1851.

[43] K.A. Gardner, L.L. Kuehnert, J.M. Mayer, Hydrogen atom abstraction by permanganate: oxidations of arylalkanes in organic solvents, Inorg. Chem. 36 (1997) 2069–2078.

[44] W.M. Latimer, The oxidation states of the elements and their potentials in aqueous solution, Second ed.Prentice-Hall Inc., New York, 1952.

[45] H.B. Gray, J.R. Winkler, Electron tunneling through proteins, Q. Rev. Biophys. 36 (2003) 341–372.

[46] H.B. Gray, J.R. Winkler, Long-range electron transfer, Proc. Natl Acad. Sci. USA 102 (2005) 3534–3539.

[47] I.-J. Chang, H.B. Gray, J.R. Winkler, High-driving-force electron transfer in metalloproteins: intramolecular oxidation of ferrocytochrome c by Ru(2, 2'-bipyridine)2(imidazole)(histidine-33)$^{3+}$, J. Am. Chem. Soc. 113 (1991) 7056–7057.

[48] H.B. Gray, J.R. Winkler, Electron flow through proteins, Chem. Phys. Lett. 483 (2009) 1–9.

[49] J. Berglund, T. Pascher, J.R. Winkler, H.B. Gray, Photoinduced oxidation of horseradish peroxidase, J. Am. Chem. Soc. 119 (1997) 2464–2469.

[50] C. Shih, A.K. Museth, M. Abrahamsson, A.M. Blanco-Rodriguez, A.J. Di Bilio, J. Sudhamsu, B.R. Crane, K.L. Ronayne, M. Towrie, A. Vlcek, J.H. Richards, J.R. Winkler, H.B. Gray, Tryptophan-accelerated electron flow through proteins, Science 320 (2008) 1760–1762.

[51] R.A. Marcus, N. Sutin, Electron transfers in chemistry and biology, Biochim. Biophys. Acta 811 (1985) 265–322.

[52] D.N. Beratan, J.N. Betts, J.N. Onuchic, Protein electron transfer rates set by the bridging secondary and tertiary structure, Science 252 (1991) 1285–1288.

[53] S.S. Skourtis, D.N. Beratan, Theories of structure–function relationships for bridge-mediated electron transfer reactions, Adv. Chem. Phys. 106 (1999) 377–452.

[54] D.N. Beratan, S.S. Skourtis, Electron transfer mechanisms, Curr. Opin. Chem. Biol. 2 (1998) 235–243.

[55] T.R. Prytkova, I.V. Kurnikov, D.N. Beratan, Coupling coherence distinguishes structure sensitivity in protein electron transfer, Science 315 (2007) 622–625.

[56] S. Hayashi, S. Kato, Solvent effect on intramolecular long-range electron-transfer reactions between porphyrin and benzoquinone in an acetonitrile solution: molecular dynamics calculations of reaction rate constants, J. Phys. Chem. A 102 (1998) 3333–3342.

[57] J.R. Miller, Reactions of trapped electrons by quantum mechanical tunneling observed by pulse radiolysis of an aqueous glass, J. Phys. Chem. 79 (1975) 1070–1078.

[58] J.R. Miller, J.V. Beitz, R.K. Huddleston, Effect of free energy on rates of electron transfer between molecules, J. Am. Chem. Soc. 106 (1984) 5057–5068.

[59] M.D. Newton, Medium reorganization and electronic coupling in long-range electron transfer, J. Electroanal. Chem. 438 (1997) 3–10.

[60] Y. Sakata, H. Tsue, M.P. O'Neil, G.P. Wiederrecht, M.R. Wasielewski, Effect of donor–acceptor orientation on ultrafast photoinduced electron transfer and dark charge recombination in porphyrin-quinone molecules, J. Am. Chem. Soc. 116 (1994) 6904–6909.

[61] K. Weidemaier, H.L. Tavernier, S.F. Swallen, M.D. Fayer, Photoinduced electron transfer and recombination in liquids, J. Phys. Chem. A 1997 (1997) 1887–1902.

[62] S.W. Swallen, K. Weidemaier, H.L. Tavernier, M.D. Fayer, Experimental and theoretical analysis of photoinduced electron transfer—including the role of liquid structure, J. Phys. Chem. 100 (1996) 8106–8117.

[63] A. Ponce, H.B. Gray, J.R. Winkler, Electron tunneling through water: oxidative quenching of electronically excited $Ru(tpy)_2^{2+}$ (tpy = 2, 2':6, 2"-terpyridine) by ferric ion in aqueous glasses at 77 K, J. Am. Chem. Soc. 122 (2000) 8187–8191.

[64] O.S. Wenger, B.S. Leigh, R.M. Villahermosa, H.B. Gray, J.R. Winkler, Electron tunneling through organic molecules in frozen glasses, Science 307 (2005) 99–102.

[65] J.F. Smalley, H.O. Finklea, C.E.D. Chidsey, M.R. Linford, S.E. Creager, J.P. Ferraris, K. Chalfant, T. Zawodzinsk, S.W. Feldberg, M.D. Newton, Heterogeneous electron-transfer kinetics for ruthenium and ferrocene redox moieties through alkanethiol monolayers on gold, J. Am. Chem. Soc. 125 (2003) 2004–2013.

[66] J.R. Winkler, D.G. Nocera, K.M. Yocom, E. Bordignon, H.B. Gray, Electron-transfer kinetics of pentaammineruthenium(III)(histidine-33)-ferricytochrome *c*. Measurement of the rate of intramolecular electron transfer between redox centers separated by 15 Å in a protein, J. Am. Chem. Soc. 104 (1982) 5798–5800.

[67] H.B. Gray, J.R. Winkler, Electron transfer in proteins, Annu. Rev. Biochem. 65 (1996) 537–561.

[68] R. Langen, I.-J. Chang, J.P. Germanas, J.H. Richards, J.R. Winkler, H.B. Gray,

Electron tunneling in proteins: coupling through a β-strand, Science 268 (1995) 1733–1735.
[69] J.J. Regan, A.J. Di Bilio, R. Langen, L.K. Skov, J.R. Winkler, H.B. Gray, J.N. Onuchic, Electron tunneling in azurin: coupling across a β sheet, Chem. Biol. 2 (1995) 489–496.
[70] J.R. Winkler, A. Di Bilio, N.A. Farrow, J.H. Richards, H.B. Gray, Electron tunneling in biological molecules, Pure Appl. Chem. 71 (1999) 1753–1764.
[71] J.R. Winkler, H.B. Gray, Electron transfer in ruthenium-modified proteins, Chem. Rev. 92 (1992) 369–379.
[72] E.T. Adman, Copper protein structures, Adv. Protein Chem. 42 (1991) 145–197.
[73] B.R. Crane, A.J. Di Bilio, J.R. Winkler, H.B. Gray, Electron tunneling in single crystals of *Pseudomonas aeruginosa* azurins, J. Am. Chem. Soc. 123 (2001) 11623–11631.
[74] J.F. Smalley, S.W. Feldberg, C.E.D. Chidsey, M.R. Linford, M.D. Newton, Y.-P. Liu, The kinetics of electron transfer through ferrocene-terminated alkanethiol monolayers on gold, J. Phys. Chem. 99 (1995) 13141–13149.
[75] O. Farver, I. Pecht, Copper proteins as model systems for investigating intramolecular electron-transfer processes, Adv. Chem. Phys. 107 (1999) 555–589.
[76] E.W. Schlag, S.Y. Sheu, D.Y. Yang, H.L. Selzle, S.H. Lin, Distal charge transport in peptides, Angew. Chem. Int. Ed. Eng. 46 (2007) 3196–3210.
[77] E. Babini, I. Bertini, M. Borsari, F. Capozzi, C. Luchinat, X. Zhang, G.L.C. Moura, I.V. Kurnikov, D.N. Beratan, A. Ponce, A.J. Di Bilio, J.R. Winkler, H.B. Gray, Bond-mediated electron tunneling in ruthenium-modified high-potential iron–sulfur protein, J. Am. Chem. Soc. 122 (2000) 4532–4533.
[78] D.N. Beratan, J.N. Onuchic, Electron tunneling pathways in proteins: influences on the transfer rate, Photosynth. Res. 22 (1989) 173–186.
[79] J.N. Onuchic, D.N. Beratan, J.R. Winkler, H.B. Gray, Pathway analysis of protein electron transfer reactions, Annu. Rev. Biophys. Biomol. Struct. 21 (1992) 349–377.
[80] I.A. Balabin, J.N. Onuchic, A new framework for electron-transfer calculations—beyond the *pathways*-like models, J. Phys. Chem. B 102 (1998) 7497–7505.
[81] K. Kumar, I.V. Kurnikov, D.N. Beratan, D.H. Waldeck, M.B. Zimmt, Use of modern electron transfer theories to determine the electronic coupling matrix elements in intramolecular systems, J. Phys. Chem. A 102 (1998) 5529–5541.
[82] S.S. Skourtis, I. Balabin, T. Kawatsu, D.N. Beratan, Protein dynamics and electron transfer: electronic decoherence and non-condon effects, Proc. Natl Acad. Sci. USA 102 (2005) 3552–3557.
[83] J.P. Lin, I.A. Balabin, D.N. Beratan, The nature of aqueous tunneling pathways between electron-transfer proteins, Science 310 (2005) 1311–1313.
[84] T. Kawatsu, D.N. Beratan, T. Kakitani, Conformationally averaged score functions for electronic propagation in proteins, J. Phys. Chem. B 110 (2006) 5747–5757.
[85] I.A. Balabin, D.N. Beratan, S.S. Skourtis, Persistence of structure over fluctuations in biological electron-transfer reactions, Phys. Rev. Lett. (2008) 101.
[86] J.J. Regan, J.N. Onuchic, Electron-transfer tubes, Adv. Chem. Phys. 107 (1999) 497–553.
[87] M.L. Tan, I. Balabin, J.N. Onuchic, Dynamics of electron transfer pathways in cytochrome *c* oxidase, Biophys. J. 86 (2004) 1813–1819.
[88] J.N. Onuchic, C. Kobayashi, K.K. Baldridge, Quantum tunneling in biological reactions: the interplay between theory and experiments, J. Braz. Chem. Soc. 19 (2008) 206–210.
[89] S.S. Skourtis, D.N. Beratan, Electron Transfer Contact Maps, J. Phys. Chem. B 101 (1997) 1215–1234.
[90] A.A. Stuchebrukhov, Tunneling currents in electron-transfer reactions in proteins. 2. Calculation of electronic superexchange matrix element and tunneling currents using nonorthogonal basis sets, J. Chem. Phys. 105 (1996) 10819–10829.
[91] A.A. Stuchebrukhov, Long-distance electron tunneling in proteins, Theor. Chem. Acc. 110 (2003) 291–306.
[92] X.H. Zheng, Y. Georgievskii, A.A. Stuchebrukhov, On the electron tunneling in molecules: a generalized orthogonalization procedure for finding tunneling orbitals, J. Chem. Phys. 121 (2004) 8680–8686.
[93] X.H. Zheng, D.M. Medvedev, A.A. Stuchebrukhov, Does internal water influence electron Tunneling in proteins? Example of cytochrome *c* oxidase, Int. J. Quant. Chem. 102 (2005) 473–479.
[94] L.D. Zusman, Outer-sphere electron transfer in polar solvents, Chem. Phys. 49 (1980) 295–304.
[95] D.F. Calef, P.G. Wolynes, Classical solvent dynamics and electron transfer. 1. Continuum theory, J. Phys. Chem. 87 (1983) 3387–3400.
[96] D.F. Calef, P.G. Wolynes, Classical solvent dynamics and electron transfer. II. Molecular aspects, J. Chem. Phys. 78 (1983) 470–482.
[97] M. Maroncelli, J. MacInnis, G. Fleming, Polar solvent dynamics and electron-transfer reactions, Science 243 (1989) 1674–1681.
[98] J.T. Hynes, Outer-sphere electron-transfer reactions and frequency-dependent friction, J. Phys. Chem. 90 (1986) 3701–3706.
[99] H. Sumi, R.A. Marcus, Dynamical effects in electron-transfer reactions, J. Chem. Phys. 84 (1986) 4894–4914.
[100] J.N. Onuchic, D.N. Beratan, J.J. Hopfield, Some aspects of electron-transfer reaction dynamics, J. Phys. Chem. 90 (1986) 3707–3721.
[101] J. Jortner, M. Bixon, Intramolecular vibrational excitations accompanying solvent-controlled electron transfer reactions, J. Chem. Phys. 88 (1988) 167–170.
[102] L. Genberg, L. Richard, G. McLendon, R.J.D. Miller, Direct observation of global protein motion in hemoglobin and myoglobin on picosecond timescales, Science 251 (1991) 1051–1054.
[103] J.S. Bashkin, G. McLendon, S. Mukamel, J. Marohn, Influence of medium dynamics on solvation and charge separation reactions: comparison of a simple alcohol and a protein "solvent", J. Phys. Chem. 94 (1990) 4757–4761.
[104] D.W. Pierce, S.G. Boxer, Dielectric relaxation in a protein matrix, J. Phys. Chem. 96 (1992) 5560–5566.
[105] S.J. Hagen, W.A. Eaton, Nonexponential structural relaxation in proteins, J. Chem. Phys. 104 (1996) 3395–3398.
[106] D.E. Khoshtariya, J. Wei, H. Liu, H. Yue, D.H. Waldeck, Charge-transfer mechanisms for cytochrome *c* adsorbed on nanometer thick films. Distinguishing frictional control from conformational gating, J. Am. Chem. Soc. 125 (2003) 7704–7714.
[107] M. Bixon, J. Jortner, Solvent relaxation dynamics and electron transfer, Chem. Phys. 176 (1993) 467–481.
[108] M. Bixon, J. Jortner, Electron transfer—from isolated molecules to biomolecules, Adv. Chem. Phys. 106 (1999) 35–202.
[109] K. Tominaga, D.A.V. Kliner, A.E. Johnson, N.E. Levinger, P.F. Barbara, Femtosecond experiments and absolute rate calculations on intervalence electron transfer of mixed-valence compounds, J. Chem. Phys. 98 (1993) 1228–1243.
[110] D.H. Son, P. Kambhampati, T.W. Kee, P.F. Barbara, Femtosecond multicolor pump-probe study of ultrafast electron transfer of $[(NH_3)_5Ru^{III}NCRu^{II}(CN)_5]^-$ in aqueous solution, J. Phys. Chem. A 106 (2002) 4591–4597.
[111] B.S. Brunschwig, C. Creutz, N. Sutin, Optical transitions of symmetrical mixed-valence systems in the Class II-III transition regime, Chem. Soc. Rev. 31 (2002) 168–184.
[112] F.W. Vance, R.V. Slone, C.L. Stern, J.T. Hupp, Comparative absorption, electro-absorption and electrochemical studies of intervalence electron transfer and electronic coupling in cyanide-bridged bimetallic systems: ancillary ligand effects, Chem. Phys. 253 (2000) 313–322.
[113] A. Ponnu, J.H. Sung, K.G. Spears, Ultrafast electron-transfer and solvent adiabaticity effects in viologen charge-transfer complexes, J. Phys. Chem. A 110 (2006) 12372–12384.
[114] C.C. Page, C.C. Moser, X. Chen, P.L. Dutton, Natural engineering principles of electron tunnelling in biological oxidation–reduction, Nature 402 (1999) 47–52.
[115] C. Aubert, M.H. Vos, P. Mathis, A.P.M. Eker, K. Brettel, Intraprotein radical transfer during photoactivation of DNA photolyase, Nature 405 (2000) 586–590.
[116] C. Tommos, G.T. Babcock, Proton and hydrogen currents in photosynthetic water oxidation, Biochim. Biophy. Acta, Bioenerg. 1458 (2000) 199–219.
[117] P.A. Frey, Importance of organic radicals in enzymatic cleavage of unactivated C–H bonds, Chem. Rev. 90 (1990) 1343–1357.
[118] W.B. Connick, A.J. Di Bilio, M.G. Hill, J.R. Winkler, H.B. Gray, Tricarbonyl(1, 10-phenanthroline)(imidazole)rhenium(I): a powerful photooxidant for investigations of electron tunneling in proteins, Inorg. Chim. Acta 240 (1995) 169–173.
[119] A. Cannizzo, A.M. Blanco-Rodríguez, A. Nahhas, J. Šebera, S. Záliš, A. Vlček Jr., M. Chergui, Femtosecond fluorescence and intersystem crossing in rhenium(I) carbonyl–bipyridine complexes, J. Am. Chem. Soc. 130 (2008) 8967–8974.
[120] A. Harriman, Further comments on the redox potentials of tryptophan and tyrosine, J. Phys. Chem. 91 (1987) 6102–6104.
[121] S. Solar, N. Getoff, P.S. Surdhar, D.A. Armstrong, A. Singh, Oxidation of tryptophan and N-methylindole by $N_3^{\cdot}$, $Br_2^{\cdot-}$, and $(SCN)_2^{\cdot-}$ radicals in light-water and heavy-water solutions—a pulse-radiolysis study, J. Phys. Chem. 95 (1991) 3639–3643.
[122] J.L. McGourty, N.V. Blough, B.M. Hoffman, Electron transfer at crystallographically known long distances (25-Å) in [Zn(II), Fe(III)] hybrid hemoglobin, J. Am. Chem. Soc. 105 (1983) 4470–4472.
[123] D. Kuila, W.W. Baxter, M.J. Natan, B.M. Hoffman, Temperature-independent electron transfer in mixed-metal hemoglobin hybrids, J. Phys. Chem. 95 (1991) 1–3.
[124] S.E. Peterson-Kennedy, J.L. McGourty, J.A. Kalweit, B.M. Hoffman, Temperature dependence of and ligation effects on long-range electron transfer in complementary [Zn, FeII]hemoglobin hybrids, J. Am. Chem. Soc. 108 (1986) 1739–1746.
[125] L.A. Dick, I. Malfant, D. Kuila, S. Nebolsky, J.M. Nocek, B.M. Hoffman, M.A. Ratner, Cryogenic electron tunneling within mixed-metal hemoglobin hybrids: protein glassing and electron-transfer energetics, J. Am. Chem. Soc. 120 (1998) 11401–11407.
[126] B. Durham, J.L. Fairris, M. McLean, F. Millett, J.R. Scott, S.G. Sligar, A. Willie, Electron transfer from cytochrome b_5 to cytochrome *c*, J. Bioenerg. Biomembr. 27 (1995) 331–340.
[127] A.G. Mauk, M.R. Mauk, G.R. Moore, S.H. Northrup, Experimental and theoretical analysis of the interaction between cytochrome *c* and cytochrome b_5, J. Bioenerg. Biomembr. 27 (1995) 311–330.
[128] M.R. Mauk, L.S. Reid, A.G. Mauk, Spectrophotometric analysis of the interaction between cytochrome b_5 and cytochrome *c*, Biochemistry 21 (1982) 1843–1846.
[129] G. McLendon, J.R. Miller, The dependence of biological electron-transfer rates on exothermicity: the cytochrome *c*/cytochrome b_5 couple, J. Am. Chem. Soc. 107 (1985) 7811–7816.
[130] L. Qin, K.K. Rodgers, S.G. Sligar, Electron transfer between cytochrome b_5 surface mutants and cytochrome *c*, Mol. Cryst. Liq. Cryst. 194 (1991) 311–316.
[131] T.E. Meyer, M. Rivera, F.A. Walker, M.R. Mauk, A.G. Mauk, M.A. Cusanovich, G. Tollin, Laser flash photolysis studies of electron transfer to the cytochrome b_5-cytochrome *c* complex, Biochemistry 32 (1993) 622–627.
[132] P. Xiong, J.M. Nocek, A.K.K. Griffin, J. Wang, B.M. Hoffman, Electrostatic redesign of the [myoglobin, cytochrome b_5] interface to create a well-defined docked complex with rapid interprotein electron transfer, J. Am. Chem. Soc. 131 (2009) 6938–6939.
[133] K. Danyal, D. Mayweather, D.R. Dean, L.C. Seefeldt, B.M. Hoffman, Conformational gating of electron transfer from the nitrogenase Fe protein to MoFe protein, J. Am. Chem. Soc. 132 (2010) 6894–6895.

[134] F.A. Tezcan, B.R. Crane, J.R. Winkler, H.B. Gray, Electron tunneling in protein crystals, Proc. Natl Acad. Sci. USA 98 (2001) 5002–5006.
[135] L. Lo Conte, C. Chothia, J. Janin, The atomic structure of protein–protein recognition sites, J. Mol. Biol. 285 (1999) 2177–2198.
[136] H. Pelletier, J. Kraut, Crystal structure of a complex between electron-transfer partners, cytochrome *c* peroxidase and cytochrome *c*, Science 258 (1992) 1748–1755.
[137] O. Miyashita, M.Y. Okamura, J.N. Onuchic, Interprotein electron transfer from cytochrome c_2 to photosynthetic reaction center: tunneling across an aqueous interface, Proc. Natl Acad. Sci. USA 102 (2005) 3558–3563.
[138] B.E. Ramirez, B.G. Malmström, J.R. Winkler, H.B. Gray, The currents of life: the terminal electron-transfer complex of respiration, Proc. Natl Acad. Sci. USA 92 (1995) 11949–11951.
[139] S. Yoshikawa, K. Shinzawa-Itoh, R. Nakashima, R. Yaono, E. Yamashita, N. Inoue, M. Yao, J.M. Fei, C.P. Libeu, T. Mizushima, H. Yamaguchi, T. Tomizaki, T. Tsukihara, Redox-coupled crystal structural changes in bovine heart cytochrome *c* oxidase, Science 280 (1998) 1723–1729.
[140] L.M. Geren, J.R. Beasley, B.R. Fine, A.J. Saunders, S. Hibdon, G.J. Pielak, B. Durham, F. Millett, Design of a ruthenium-cytochrome *c* derivative to measure electron transfer to the initial acceptor in cytochrome *c* oxidase, J. Biol. Chem. 270 (1995) 2466–2472.
[141] L.P. Pan, S. Hibdon, R.-Q. Liu, B. Durham, F. Millett, Intracomplex electron transfer between ruthenium-cytochrome *c* derivatives and cytochrome *c* oxidase, Biochemistry 32 (1993) 8492–8498.
[142] V.A. Roberts, M.E. Pique, Definition of the interaction domain for cytochrome *c* on cytochrome *c* oxidase. III. Prediction of the docked complex by a complete systematic search, J. Biol. Chem. 274 (1999) 38051–38060.
[143] D. Flöck, V. Helms, Protein–protein docking of electron transfer complexes: cytochrome *c* oxidase and cytochrome *c*, Proteins: Struct. Func. Gen. 47 (2002) 75–85.
[144] H. Witt, F. Malatesta, F. Nicoletti, M. Brunori, B. Ludwig, Tryptophan 121 of subunit II is the electron entry site to cytochrome-c oxidase in *Paracoccus denitrificans*—involvement of a hydrophobic patch in the docking reaction, J. Biol. Chem. 273 (1998) 5132–5136.
[145] Y.J. Zhen, C.W. Hoganson, G.T. Babcock, S. Ferguson-Miller, Definition of the interaction domain for cytochrome c on cytochrome c oxidase—I. Biochemical, spectral, and kinetic characterization of surface mutants in subunit II of *Rhodobacter sphaeroides* cytochrome aa_3, J. Biol. Chem. 274 (1999) 38032–38041.
[146] K.F. Wang, Y.J. Zhen, R. Sadoski, S. Grinnell, L. Geren, S. Ferguson-Miller, B. Durham, F. Millett, Definition of the interaction domain for cytochrome *c* on cytochrome c oxidase - II. Rapid kinetic analysis of electron transfer from cytochrome c to *Rhodobacter sphaeroides* cytochrome oxidase surface mutants, J. Biol. Chem. 274 (1999) 38042–38050.
[147] V. Drosou, F. Malatesta, B. Ludwig, Mutations in the docking site for cytochrome c on the Paracoccus heme aa_3 oxidase—electron entry and kinetic phases of the reaction, Eur. J. Biochem. 269 (2002) 2980–2988.
[148] S.D. George, M. Metz, R.K. Szilagyi, H. Wang, S.P. Cramer, Y. Lu, W.B. Tolman, B. Hedman, K.O. Hodgson, E.I. Solomon, A quantitative description of the ground-state wave function of Cu_A by X-ray absorption spectroscopy: comparison to plastocyanin and relevance to electron transfer, J. Am. Chem. Soc. 123 (2001) 5757–5767.
[149] O. Farver, O. Einarsdóttir, I. Pecht, Electron transfer rates and equilibrium within cytochrome *c* oxidase, Eur. J. Biochem. 267 (2000) 950–954.
[150] J.J. Regan, B.E. Ramirez, J.R. Winkler, H.B. Gray, B.G. Malmström, Pathways for electron tunneling in cytochrome *c* oxidase, J. Bioenerg. Biomembr. 30 (1998) 35–39.
[151] D.R. Gamelin, D.W. Randall, M.T. Hay, R.T. Houser, T.C. Mulder, G.W. Canters, S. de Vries, W.B. Tolman, Y. Lu, E.I. Solomon, Spectroscopy of mixed-valence Cu_A-type centers: ligand-field control of ground-state properties related to electron transfer, J. Am. Chem. Soc. 120 (1998) 5246–5263.
[152] D.M. Medvedev, I. Daizadeh, A.A. Stuchebrukhov, Electron transfer tunneling pathways in bovine heart cytochrome *c* oxidase, J. Am. Chem. Soc. 122 (2000) 6571–6582.
[153] R.H. Goldsmith, L.E. Sinks, R.F. Kelley, L.J. Betzen, W. Liu, E.A. Weiss, M.A. Ratner, M.R. Wasielewski, Wire-like charge transport at near constant bridge energy through fluorene oligomers, Proc. Natl. Acad. Sci. USA 102 (2005) 3540–3545.
[154] E. Yavin, A.K. Boal, E.D.A. Stemp, E.M. Boon, A.L. Livingston, V.L. O'Shea, S.S. David, J.K. Barton, Redox activation of a DNA repair protein by guanine radical, Proc. Natl. Acad. Sci. USA 102 (2005) 3546–3551.